Journal of Hazardous Materials 177 (2010) 639–647

Contents lists available at ScienceDirect

Journal of Hazardous Materials

journal homepage: www.elsevier.com/locate/jhazmat

Preparation of silver-modified TiO_2 via microwave-assisted method and its photocatalytic activity for toluene degradation

Xiaobin Li, Linling Wang, Xiaohua Lu*

Environmental Science Research Institution, Huazhong University of Science and Technology, No. 1037 Luoyu Road, Wuhan 430074, PR China

ARTICLE INFO

Article history:
Received 2 September 2009
Received in revised form
26 November 2009
Accepted 16 December 2009
Available online 24 December 2009

Keywords:
Ag
TiO_2
Microwave-assisted
Photocatalytic activity
Gaseous toluene

ABSTRACT

Silver-modified TiO_2 (Ag-TiO_2) with various Ag/Ti molar ratios were prepared by the microwave-assisted method and characterized by X-ray diffraction (XRD), transmission electron microscope (TEM) and UV–vis diffuse reflectance spectroscopy (UV–vis-DRS). Compared with the hydrothermal method, Ag-TiO_2 of small crystallite size and high crystallinity can be obtained by the microwave-assisted preparation method. When the Ag/Ti molar ratio increased from 0 to 2%, the doping of Ag promoted the phase transformation and inhibited the growth of anatase crystallite. The absorption edge of Ag-TiO_2 shifted to longer wavelength, and the band gap energy of Ag-TiO_2 decreased. However, after increasing the molar ratio Ag/Ti further from 2 to 4%, the anatase content, the crystallite size and the band gap energy of Ag-TiO_2 only increased slightly. In photodegradation gaseous toluene, the photocatalytic activity of Ag-TiO_2 increased with the increase of Ag/Ti molar ratio from 0 to 1%, but declined with the further increase to 2%. The optimal Ag/Ti molar ratio for photocatalytic activity of Ag-TiO_2 was found as 1%, with the content of anatase, rutile and brookite of 71.1, 14.5 and 14.4%, respectively. Compared with TiO_2, Ag-TiO_2 exhibited a better photostability in toluene degradation.

1. Introduction

The use of heterogeneous photocatalysis in the degradation of environment pollutants has aroused intensive attention during the past two decades [1,2]. Among various semiconductor photocatalysts for environment purification, titania appears to be the most promising and important one due to its stable physical and chemical characteristics, unique electronic properties, strong oxidizing power, non-toxicity and low price [3]. However, the wide band gap of TiO_2 (>3.0 eV) [4] and the high recombination rate of the photoinduced electron–hole pairs formed in photocatalytic processes [2] limit the efficiency of the photocatalytic degradation of toxicants.

Doping TiO_2 with noble metals, such as Pt [5], Pd [6] and Au [7], can overcome the aforementioned deficiency. However, these noble metals are too expensive to be utilized in industrial scale. Compared with Au, Pd and Pt, Ag is for less expensive and deserves further investigation. Ag can act as an electron trap and promote the interfacial charge transfer processes in the composite systems, which reduces the recombination of the photoinduced electron–hole pairs, thus improving the photocatalytic activity of TiO_2 [8,9]. Sung-Suh and Li [10,11] have found that Ag can broaden the adsorption edge of TiO_2 and improve its photocatalytic activity in the visible region. Besides, Ag has also been observed to play an important role in increasing the photocatalytic stability of TiO_2 [12], suggesting that the photocatalytic activity of Ag-TiO_2 depends mainly on the uniformity of Ag dispersion on the TiO_2 surface and the microstructure and phase of TiO_2. Furthermore, as the characteristics and structure of photocatalysts was different when using preparation processes, the preparation method plays a key role in a successful synthesis of catalysts.

However, the conventional preparation methods still have some disadvantages. For example, the hydrothermal method and ultrasonic-assisted sol–gel technique [13] require a long synthesis time and high calcining temperature, which results in the aggregation of particles; the photoreduction method cannot make a satisfactorily dispersion of Ag particles on the surface of TiO_2, which markedly decreases the amount of active sites on the surface of TiO_2 [14]. Recently a new improved method named, microwave-assisted preparation method (MW), has attracted much interest [15]. Hart et al. [16] have compared the microwave and conventional heat treatments in preparing nanocrystalline TiO_2 and found that the microwave heating promoted the phase transformation of TiO_2 from anatase to rutile. They have suggested that microwave may offer a clean, faster, cost effective and convenient method of heating. Similar results have also been obtained by Liu et al. [17] in the preparation of Pt modified TiO_2. They found that the Pt nanoparticles were uniformly dispersed on TiO_2 particles during the microwave-heating process, which improved the photocatalytic activity of TiO_2/Pt. Guo et al. [18] have prepared

* Corresponding author. Tel.: +86 27 87792159; fax: +86 27 87792159.
E-mail address: hust-esri2009@hotmail.com (X. Lu).

0304-3894/$ – see front matter © 2009 Elsevier B.V. All rights reserved.
doi:10.1016/j.jhazmat.2009.12.080

Ag/TiO_2-nanotubes by MW, which has shown a high photocatalytic activity in the degradation of organochlorine pesticides. However, these previous studies have not addressed the influence of Ag on the microstructure and phase transformation of TiO_2 under microwave irradiation, which may play important role in improving the photocatalytic activity of TiO_2.

In this study, Ag-modified TiO_2 powders with various Ag/Ti molar ratios were prepared by MW. The microstructure, photocatalytic activity and photostability of the prepared catalysts were investigated via characterizing the catalysts by XRD, TEM and UV–vis-DRS. The photocatalytic degradation of toluene, one of the typical volatile organic compounds indoors, was used to evaluate the photocatalytic activity of prepared photocatalysts.

2. Experimental

2.1. Materials

Tetra-*n*-butyl titanate ($Ti(OBu)_4$, >99.9%) and silver nitrate ($AgNO_3$, analytical grade) were purchased from Aldrich and used as titanium and silver sources, respectively. Other chemicals were from Shanghai Chemical Regent Factory of China without further purification. For the preparation of TiO_2 and Ag-modified TiO_2 photocatalysts, ethanol (C_2H_5OH, chemical reagent) was used as solvent. Toluene (C_7H_8, chemical reagent) was used as a source of gaseous toluene.

2.2. Preparation of photocatalysts

TiO_2 was prepared by conventional sol–gel method. 10 mL of $Ti(OBu)_4$ was added into 17.5 mL of ethanol, and the solution was dispersed by ultrasound for 10 min. Then the solution was added dropwise (about 1 mL/min) into the mixed solution containing 10.5 mL of deionized water and 17.5 mL of ethanol. The mixture was continuously stirred for 2 h, and the resultant solution was aged for 24 h at room temperature. The TiO_2 sol obtained was dried at 65 °C for 12 h, and the powder was washed with ethanol and water for three times. Then the TiO_2 xerogel was obtained.

A certain amount of TiO_2 xerogel was poured into 20 mL of $AgNO_3$ solution with Ag/Ti molar ratios of 0, 0.01, 0.25, 0.5, 1, 2 and 4%. The solution was transferred to a Teflon vessel (27 mL), and irradiated by microwave in the Microwave Digestion/Extraction system (SINEO Co. Ltd, Shanghai) at 600 W, 150 °C and 0.5 MPa for 30 min. The vessel was naturally cooled to room temperature. After centrifugation at 4500 rpm for 15 min, the final precipitate was washed with deionized water and ethanol, and then dried under vacuum at 65 °C for 12 h. The samples with Ag/Ti molar ratios of 0, 0.01, 0.25, 0.5, 1, 2 and 4% were denoted as WT, 0.01, 0.05, 0.25, 0.5, 1, 2 and 4%AgWT, respectively. For comparison, the Ag-modified TiO_2 (Ag/Ti molar ratio of 1%) was also prepared by hydrothermal method. The preparing process was the same as that of WT, except that the Teflon vessel with TiO_2 xerogel and $AgNO_3$ solution was heated in muffle at 150 °C for 30 min and 24 h, respectively. The prepared samples were denoted as a-1%AgHT and b-1%AgHT.

2.3. Characterization of photocatalysts

The crystalline phase of the catalysts were analyzed by X-ray powder diffraction (XRD) using a X'Pert PRO X-ray diffractometer equipped with a Cu Kα radiation ($\lambda = 0.15406$ nm). The accelerating voltage of 40 kV and emission current of 40 mA were used. The particles were spread on a glass slide specimen holder and the scattered intensity was measured between 20° and 80° at a scanning rate of $2\theta = 5°$/min. The average crystallite sizes of anatase were determined according to the Scherrer formula using the FWHW data of each phase after correcting the instrumental broadening [19]. The phase composition of sample could be obtained from the integrated intensities of anatase (1 0 1), rutile (1 1 0) and brookite (1 2 1) peaks. The mass fraction of anatase (W_A), rutile (W_R) and brookite (W_B) could be calculated from equations according to the methods previously reported [20].

The texture and morphology of samples were studied using a FEI Quanta 200 Transmission electron microscope (TEM) and a JEOL TEM-2010F high-resolution transmission electron microscopy (HRTEM) with an accelerating voltage of 200 kV. A sample was deposited onto a copper grid after being dispersed in methanol by an ultrasonic bath.

UV–vis diffuse reflectance spectroscopy (UV–vis-DRS) in the spectral range from 800 to 190 nm was performed with a Lambda 35 UV–vis spectrometer (PerkinElmer). The presented spectra are the average of three separate scans performed at a speed of 120 nm/min with a bandwidth of 2 nm. The baseline correction was performed using a calibrated reference sample of barium sulfate.

2.4. Experimental procedure of photocatalytic degradation of toluene

The photocatalytic degradation of gaseous toluene was carried out in a Pyrex glass cylindrical reactor with a diameter of 80 mm and an effective volume of 2 L. A 28 W ultraviolet lamp with wavelength of 254 nm (Cnlight, Co. Ltd., China) was installed in the middle of reactor as light source. The reaction temperature was controlled at 25 °C by air-condition system. A specified amount of photocatalyst (1.5 g) was dispersed on stainless steel net with 300 mesh (a length of 600 mm, a width of 400 mm) adhered on the inner wall of reactor. The surface features of stainless steel net before and after spraying catalysts are shown in Fig. 1. It can be seen that the catalyst powders are homogeneously dispersed on the surface of stainless steel net.

The saturated toluene gas was prepared by passing air through a thermostated saturator containing liquid toluene. The obtained toluene gas stream entered the photoreactor at a flow rate 1.5 L/min. The initial toluene concentration in reactor was controlled at 9.0 ± 0.5 mg/L. Prior to photodegradation, toluene was adsorbed on the photocatalyst without illumination for 30 min. Then the light was turned on to initiate the reaction. The similar experiments of the photocatalytic degradation of toluene were also performed under the visible light irradiation (a wavelength of 410 nm).

2.5. Analytical method

The gas samples were collected periodically using a glass injector (25 mL), and monitored by a gas chromatograph (Fuli 9790, China) equipped with an FID detector and a PEG-20000 column (a length of 2 m and a diameter of 3 mm). N_2 was used as carrier gas and the flow rate was 30 mL/min. The inlet temperature was 100 °C, the oven temperature was 80 °C, and the detector temperature was 250 °C. The gas samples were injected in GC via a six-way valve, and the injection volume was 1 mL.

To analyze the by-products and remaining reactant adsorbed on the surface of catalyst, 1 g of catalyst powders (WT or 1%AgWT) were dispersed uniformly on the surface of glass slide (a length of 50 mm, a width of 30 mm), and placed in the middle of reactor. The experiments for toluene degradation were repeatedly carried out in the above-mentioned reaction condition for eight runs. Accumulated intermediate organic products and remaining reactant were extracted from the WT and 1%AgWT by 5 mL carbon disulfide assisted by 10 min ultrasonication.

Qualitative analysis of the filtrate was carried out by an GC (Varian 3900 Gas Chromatograph) equipped with a CP-SIL 24CB LOWBLEED-MS capillary column (a length of 30 m, a diameter of 0.25 mm, a film thickness of 0.25 μm) and a MS (Saturn 2100T mass

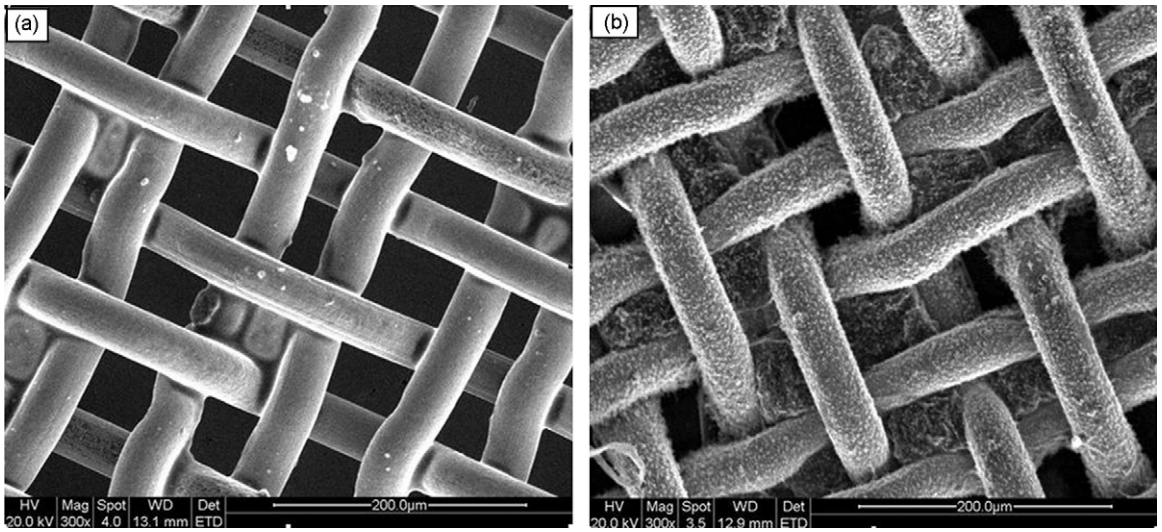

Fig. 1. SEM picture catalyst films: (a) stainless steel net with 300 meshes; (b) TiO_2 on stainless steel net.

analyzer detector). The inlet temperature and the detector temperature was 180 and 250 °C, respectively. The temperature program started at 40 °C for 2 min, and then increased to 260 °C at a rate of 10 °C/min and kept for 10 min. Helium was served as the carrier gas at a flow rate of to 1.7 mL/min. The injection volume was 1 μL.

3. Results and discussion

3.1. Characterization of photocatalysts

3.1.1. XRD analysis

Fig. 2 shows the XRD patterns of a-1%AgHT, b-1%AgHT, 1%AgWT and WT. The diffraction peaks at $2\theta = 25.3°$, 37.8°, 48.2°, 54.4° and 62.9° are attributed to anatase phase of TiO_2, and the diffraction peaks at $2\theta = 27.3°$ and 30.7° are assigned to rutile and brookite phase of TiO_2, respectively. It can be seen that the high crystallinity of TiO_2 was obtained in b-1%AgHT and 1%AgWT, while no phase diffraction peak was observed in a-1%AgHT. This difference indicated that the crystallite TiO_2 powders were not formed in a short hydrothermal time, but formed in a short microwave irradiation time. Interestingly, WT consisted of pure anatase without other phases. After doping TiO_2 with Ag, two new phases (rutile and brookite) were observed in 1%AgWT and b-1%AgHT, respectively. It can be deduced that Ag promoted the TiO_2 phase transformation from anatase to other phases. In addition, the crystallite sizes of samples (shown in Table 1), calculated using Scherrer formula from the main anatase diffraction peaks, were in the order of WT > 1%AgHT > 1%AgWT. This means that Ag-modified TiO_2 (Ag-TiO_2) with small crystallite size and high crystallinity can be prepared by MW.

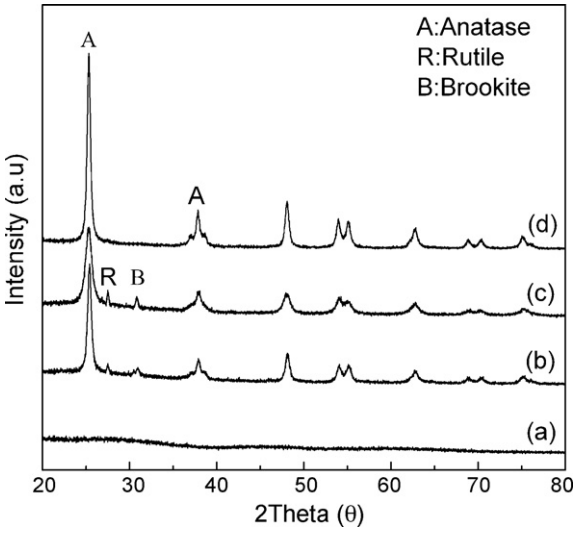

Fig. 2. XRD patterns of Ag-modified TiO_2 prepared by different methods: (a) a-1%AgHT; (b) b-1%AgHT; (c) 1%AgWT; (d) WT.

In a microwave-heated system, the microwave power was dissipated over the entire volume of solvent, where nucleation points necessary for boiling were absent [21]. The average temperature of the solvent was significantly higher than the atmospheric boiling temperature. Boiling only occurred at the reactor walls or at the solvent–air interface. This resulted in a reversed temperature profile with a steady average reflux temperature above the classical boiling point. As a result, chemical reactions proceed more quickly than that using conventional heating [22]. Thus, high crystallinity of TiO_2 was obtained by microwave heating in a short time. Furthermore, Ag has a very strong heating response to microwave [23]. In the microwave-heating system, the localized heating around Ag particles increased drastically, which probably provided enough energy for the phase transformation from anatase to other phase. This may be a reason that the rutile and brookite phase content of 1%AgWT were larger than that of b-1%AgHT. Interestingly, the crystalline size of 1%AgWT was smaller than that of b-1%AgHT in spite of the presence of higher localized heating in the preparation process of 1%AgWT. This confliction can be attributed to the facts as follows. On the one hand, the more Ag particles on the surface of TiO_2, the higher the increase of localized heating, which enhanced the growth of the crystallite size. Therefore, the crystalline size of the catalyst increased with the increase of Ag/Ti molar ratio from 0 to 2%. On the other hand, the longer heating time is in favor of the crystalline size of TiO_2. In this work, the heating time (i.e., 24 h) for the preparation of b-1%AgHT was much longer than that for 1%AgWT (30 min). We propose that the heating time played a key role in the crystalline size of TiO_2 in our investigation.

Fig. 3 compares the XRD patterns of Ag-TiO_2 powders with different Ag/Ti molar ratios prepared by MW. The average crystallite sizes are included in Table 1. Anatase phase was observed in all the XRD patterns of samples. The peak intensity and the crystallite size of anatase decreased with the increase of the Ag/Ti molar ratio from 0 to 2%, but increased slightly when the Ag/Ti molar ratio rose to 4%, indicating that the appropriate doping amount of Ag inhibited the

Table 1
Effects of molar ratio of Ag/Ti on average crystallite size, phase content, diffraction angle, and bang gap of Ag-modified TiO_2.

Sample	Crystallite size(nm)	Phase content (%)			Diffraction angle (°)	E_g (eV)
		Anatase	Rultile	Brookite		
WT	24.3	100	–	–	25.60	3.12
0.05AgWT	22.7	100	–	–	25.48	3.08
0.25AgWT	20.1	100	–	–	25.40	3.05
0.5AgWT	17.4	80.8	7.9	11.2	25.38	3.02
1AgWT	13.3	71.1	14.5	14.4	25.27	2.98
2AgWT	10.2	40.3	17.3	42.4	25.21	2.91
4AgWT	11.6	40.5	15.1	44.4	25.32	2.94
a-1AgHT	–	–	–	–	–	–
b-1AgHT	14.5	79.9	7.8	2.3	25.30	3.00

growth of anatase grains. The observations can be explained by facts as follows. (a) As the high heat and pressure were generated in the pore of TiO_2 xerogel instantly during microwave irradiation, more Ag^+ ions migrated from the pore of TiO_2 xerogel particles to their surface and further to the surface of TiO_2 along the grain boundaries with water molecules and other impurities. The diffusion and rearrangement of Ti^+ and O^{2-} ions in anatase grain boundaries would be greatly disturbed and inhibited by these larger Ag^+ ions. The mutual contact and material transfer between anatase grains were also hindered. The necessary energy for the movement of anatase grain boundary then increased, while the driving force for anatase grain boundary migration decreased, which caused a slower grain growth rate and smaller particle size [24]. (b) Excess Ag^+ ions led to the further increase of densities of defects and anion vacancies on the surface of anatase grains, which would promote the sintering of anatase grains, and result in larger anatase grains [24]. As a consequence, the particles size of 4%AgWT was larger than that of 2%AgWT.

In addition, it can be found that with the Ag/Ti molar ratio above 0.5%, rutile and brookite appeared in Ag-TiO_2, and the peak intensity of rutile and brookite increased. Firstly, the density of surface defects and surface oxygen vacancy concentration of anatase grains increased with the increase of Ag doping content, which favored the rearrangement of ions and reorganization of structure for rutile [24,25], and promoted the phase transformation. It have been reported that Ag^+ ions can catalyze the transformation from anatase to brookite [26]. Furthermore, in microwave-heating system, the decomposition of $AgNO_3$ (reactions (1)–(3)) released thermal energy, which had a positive effect on the phase transformation [20]:

$$AgNO_3 \xrightarrow{T} Ag_2O + N_2O + NO \quad (1)$$

$$Ag_2O \xrightarrow{T} Ag + O_2 \quad (2)$$

$$nAg \rightarrow (Ag)_n \quad (3)$$

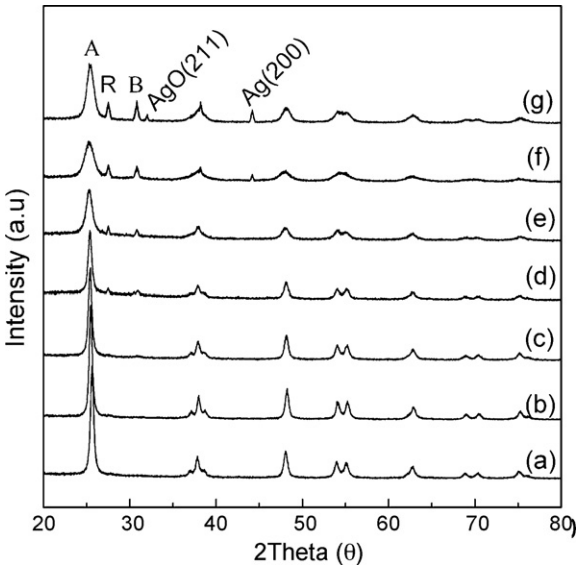

Fig. 3. XRD patterns of Ag-modified TiO_2 at different Ag/Ti molar ratios: (a) WT; (b) 0.05%AgWT; (c) 0.25%AgWT; (d) 0.5%AgWT; (e) 1%AgWT; (f) 2%AgWT; (g) 4%AgWT. Where A, R and B indicate anatase, rutile and brookite phase, respectively.

When the Ag/Ti molar ratio was above 2%, two new diffraction peaks assigned to Ag (1 1 1) and Ag (2 0 0) appeared at $2\theta = 38.4°$ and 44.2°, respectively. However, due to the strong diffraction peak of anatase (at $2\theta = 37.8$) and low amounts of Ag (1 1 1), the peak at $2\theta = 38.4°$ was not clearly observed. When the Ag/Ti molar ratio increased to 4%, the diffraction peaks for AgO (2 1 1) appeared at $2\theta = 31.4°$, which was probably attributed to the oxidation of Ag to AgO.

As shown in Fig. 3, we also observed that the XRD position of anatase (1 0 1) shifted to low angle with the increase of Ag/Ti molar ratio from 0 to 2%. According to Bragg's law, the less the value of $\sin\theta$, the larger the d spacing. Xin et al. [9] concluded that the value of d spacing was gradually increased with the increase of Ag content. However, because the ionic radius of Ag^+ (ca. 126 pm) is larger than that of Ti^{4+} (ca. 68 pm), Ag^+ cannot diffused into the lattice of TiO_2 [27]. We propose that the value of d spacing was gradually increased with the decrease in the anatase crystallite size. When the Ag/Ti molar ratio rose to 4%, the XRD position slightly rose, and the anatase crystallite size was larger than that of 2%AgWT. This also implies that the value of d spacing depended on the crystallite size.

3.1.2. TEM observation

Fig. 4 shows the TEM images of a-1%AgHT, b-1%AgHT, WT and 1%AgWT. It can be seen that all the TEM images of b-1%AgHT, WT and 1%AgWT except a-1%AgHT showed clear crystal shapes. The crystallite size of b-1%AgHT, WT and 1%AgWT were from 16 to 27 nm, from 19 to 37 nm and from 13 to 22 nm, respectively, which agreed well with the results of XRD (shown in Table 1). As expected, the Ag clusters were observed in Fig. 4b, and the average particles size was about 5 nm. Fig. 4e shows a high-resolution transmission electron microscopy (HRTEM) image of 4%AgWT particles. The lattice planes of anatase (1 0 1), rutile (1 1 0), brookite (1 1 1), Ag (1 1 1) and AgO (2 1 1) with interlayer spacing of 0.356, 0.324, 0.346, 0.240 and 0.278 nm, respectively, were clearly displayed. Five phase particles were in close contact with each other. This close interconnection was supposed to favor the photoinduced electrons transfer between the phases [20], which reduced the recombination of the photoinduced electrons and holes, and improved the photocatalytic activity of catalysts.

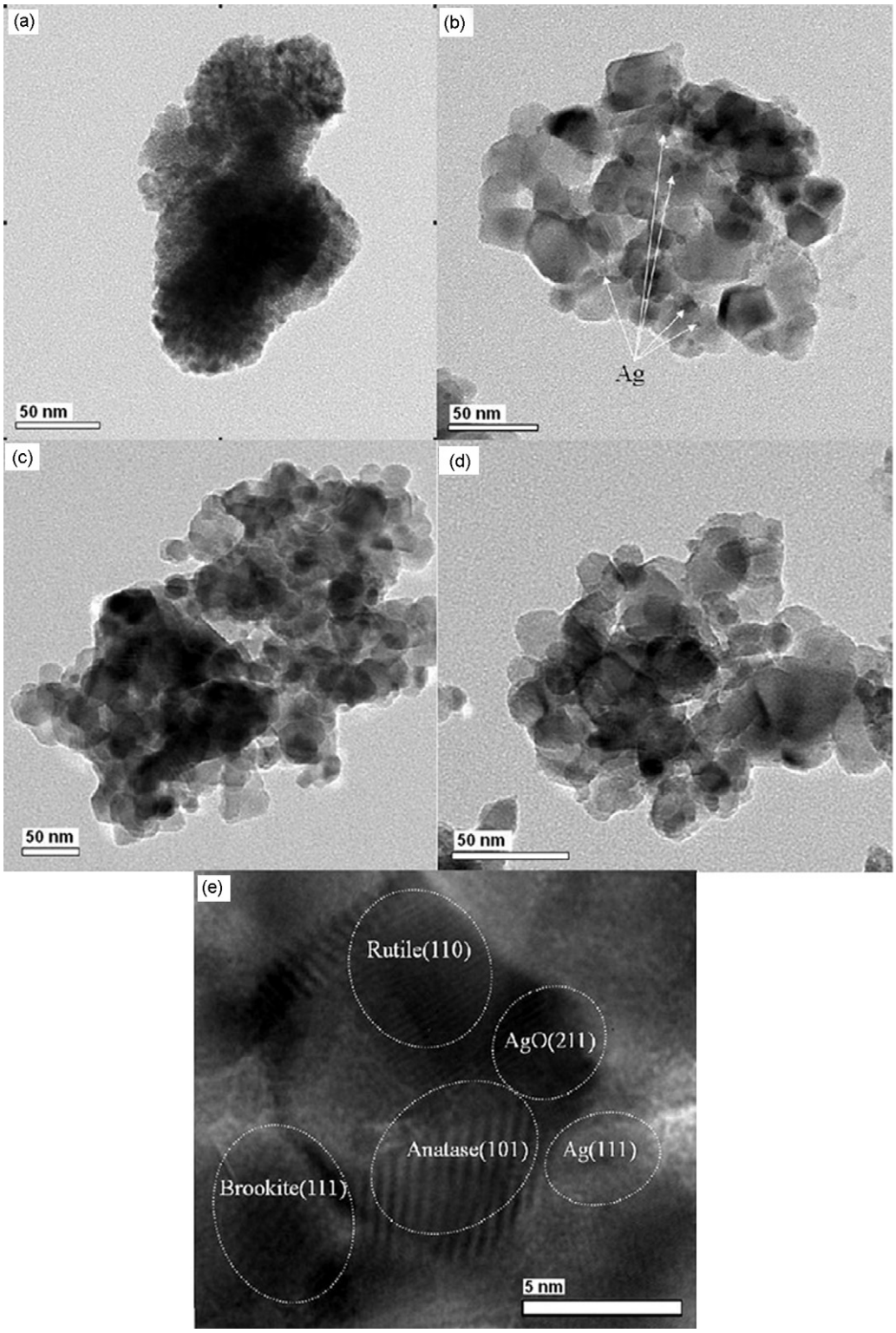

Fig. 4. TEM images of Ag-modified TiO_2: (a) a-1%AgHT; (b) 1%AgHT; (c) 1%WT; (d) 1%AgWT; (e) 4%AgWT.

3.1.3. UV–vis spectra

The diffuse reflectance UV–vis spectra of WT, b-1%AgHT and 1%AgWT are displayed in Fig. 5. The UV–vis spectra of all samples demonstrated strong absorption in UV light region. Compared with WT, the absorption edges (λ_g) of b-1%AgHT and 1%AgWT shifted to longer wavelength, indicating that doping TiO_2 with Ag broadened the absorption edge of TiO_2. The band gap energy (E_g) of WT, b-1%AgHT and 1%AgWT were 3.12, 3.00 and 2.98 eV, respectively (Table 1). Herein, the band gap energies of samples were determined from the equation, $E_g = 1239.8/\lambda$ [28], where λ is the wavelength (nm) of the exciting light. The band gap energy of 1%AgWT was smaller than that of b-1%AgHT as the crystallite size of b-1%AgHT was larger than that of 1%AgWT, agreeing with the report by Li et al. [29]. In addition, a new absorption band at 525 nm appeared in 1%AgWT and b-1%AgHT (Fig. 5a and b), which was attributed to the surface plasmon absorption of spatially confined

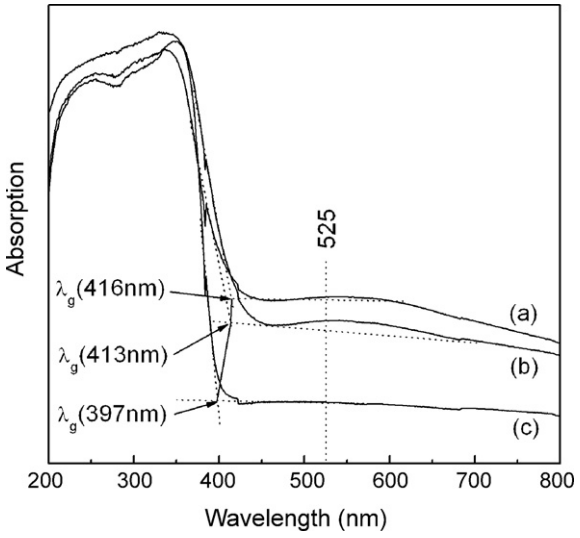

Fig. 5. Diffuse reflectance UV–vis spectras of Ag-modified TiO_2 by different preparation methods: (a) 1%AgWT; (b) b-1%AgHT; (c) WT.

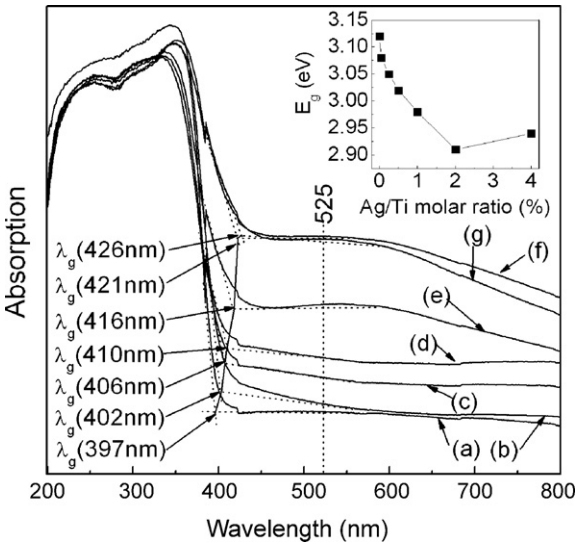

Fig. 6. Diffuse reflectance UV–vis spectras of Ag-modified TiO_2 at different molar ratio of Ag/Ti: (a) WT; (b) 0.05%AgWT; (c) 0.25%AgWT; (d) 0.5%AgWT; (e) 1%AgWT; (f) 2%AgWT; (g) 4%AgWT. The inset shows the relation between the band gap and the molar ratio of Ag/Ti.

electrons in Ag nanoparticles. Compared with the typical plasmon peak of Ag nanoparticles at 400 nm, these absorption bands had a large shift, which was assigned to the high refractive index of the TiO_2 and interaction between Ag and TiO_2 [30].

The effect of Ag doping content on the absorption edge and the band gap energy of TiO_2 were also investigated with diffuse reflectance spectroscopy. The results are shown in Fig. 6. The inset displays the effect of Ag doping content on the band gap of samples. It can be seen that the absorption edge of samples shifted towards longer wavelength significantly and the absorption in visible light region became strong after doping TiO_2 with Ag. The band energy of samples decreased with the increase of Ag/Ti molar ratio from 0 to 2%, and then slightly declined with the further increase of Ag/Ti molar ratio above 2% (shown in Table 1). The absorption peak at the center of 525 nm was also observed in Ag-TiO_2 catalysts, and its intensity increased with the increase of Ag/Ti molar ratio. This suggested that Ag nanoparticle size was increased and/or the size distribution became wide with the increase of Ag/Ti molar ratio [31]. The peak intensity of 4%AgWT at 525 nm was similar to that of 2%AgWT, indicating that Ag nanoparticle size was no longer being increased when the Ag/Ti molar ratio was above 2%.

3.2. Adsorption and photocatalytic activities of photocatalysts

To investigate the influence of the preparation methods and Ag content on the photocatalytic activity of Ag-TiO_2, the photocatalytic degradation of toluene on the prepared samples were compared. Prior to UV light irradiation, the photocatalysis system was placed in dark for the adsorption saturation of toluene on the samples. The photocatalytic degradation experiments without catalyst (data not shown) resulted in a negligible decrease in toluene concentration (below 4.7%) during the 3 h UV irradiation applied.

Fig. 7(A) shows the photocatalytic degradation curves of gaseous toluene on WT, a-1%AgHT, b-1%AgHT and 1%AgWT under UV light irradiation, respectively. The concentration of toluene in reactor declined slightly in dark and drastically declined after 3 h UV irradiation, indicating that the photodegradation of toluene depend on the present of both UV light irradiation and catalysts. The a-1%AgHT showed a poor photocatalytic activity due to its low degree of crystallinity. The degradation rate of toluene on 1%AgWT and b-1%AgHT were higher than that on WT, indicating that the photocatalytic activity of catalyst was improved after doping TiO_2 with Ag. The degradation rate of toluene on the b-1%AgHT was smaller than that on 1%AgWT, probably due to the influence of microstructure, which was changed by the different preparation methods, on the photocatalytic activity of TiO_2. The similar experiments were performed under the visible light irritation (Fig. 7(B)). However, 1%AgWT and b-1%AgHT exhibited the higher visible photocatalytic activity compared with WT and a-1%AgHT, which provided

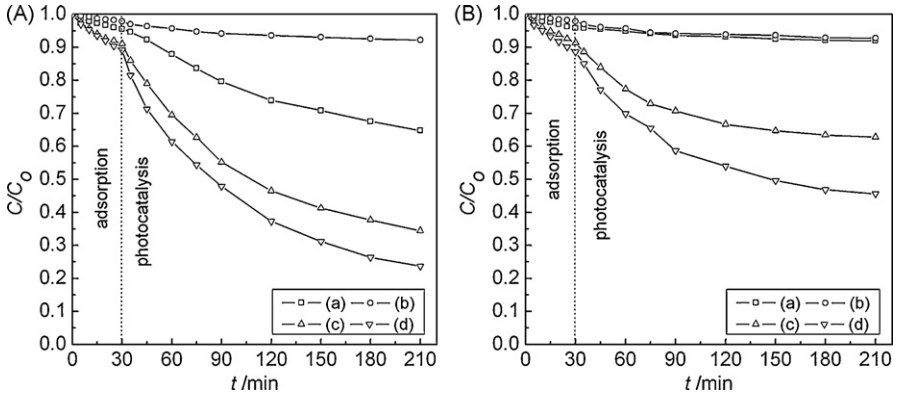

Fig. 7. Kinetics curves of gaseous toluene photocatalytic degradation on the catalysts prepared by different preparation methods under UV light (A) and visible light (B) irradiation. (a) WT; (b) a-1%AgHT; (c) b-1%AgHT; (d) 1%AgWT.

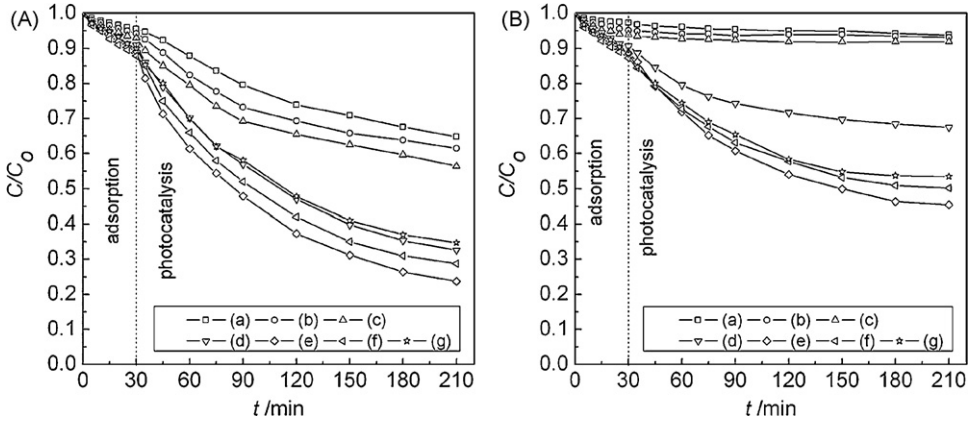

Fig. 8. Kinetics curves of gaseous toluene photocatalytic degradation on Ag-modified TiO_2 under UV light (A) and visible light (B) irradiation at different molar ratio of Ag/Ti: (a) WT; (b) 0.05%AgWT; (c) 0.25%AgWT; (d) 0.5%AgWT; (e) 1%AgWT; (f) 2%AgWT; (g) 4%AgWT.

negligible degradation of toluene. This was probably due to the low absorption edge (resulted in the analysis of UV–vis-DRS) of Ag-modified TiO_2.

Fig. 8(A) and (B) shows the effect of Ag/Ti molar ratio on the adsorption and the photocatalytic activity of Ag-TiO_2. Under UV irradiation, the photocatalytic activity of Ag-TiO_2 were in the order of 1%AgWT > 2%AgWT > 4%AgWT > 0.5%AgWT > 0.25%AgWT > 0.05%AgWT > WT. Under visible light irradiation, the photocatalytic degradation of toluene was negligible on WT, 0.05 and 0.25%AgWT, but obvious on 0.5, 1, 2 and 4%AgWT, suggesting that the increase of Ag content was in favor of the photocatalytic application of TiO_2 under visible light irradiation. The Ag/Ti molar ratio at 1% provided the highest efficiency for toluene photodegradation on Ag-TiO_2 powders, indicating that an appropriate Ag doping content could improve the photocatalytic activity of catalysts.

The crystallite size plays an important role in the photocatalytic activity of TiO_2. A smaller crystallite size led to a larger photoactive area, and therefore, a higher photocatalytic activity [32]. Herein, when the Ag/Ti molar ratio increased from 0 to 1%, the photocatalytic activity of Ag-TiO_2 was enhanced with the decrease of its crystallite size (Table 1, Figs. 7 and 8). When the Ag/Ti molar ratio rose to above 2%, the crystallite size of Ag-TiO_2 further decreased while the photocatalytic activity of catalysts dropped. This conflict suggests that the crystallite size is not the determining factor.

The dominant factors for the photocatalytic activity of Ag-TiO_2 may be related to the formation of Schottky barriers between anatase and the other phases. In the low Ag doping content (Ag/Ti molar ratio from 0 to 0.25%), the catalysts contained only anatase phase. The photocatalytic activity of Ag-TiO_2 depended on the crystallite size of anatase, and showed a slight shift in the degradation of toluene. When the Ag/Ti molar ratio rose from 0.5 to 2%, the catalysts consisted of anatase, rutile, brookite and/or Ag (Fig. 4), and these phases were in close contact, which formed many hetero-junctions such as anatase/rutile, anatase/brookite, Ag/anatase and Ag/rutile [20]. Under UV light irradiation, the electrons were moved between the phases (from high Fermi level to low Fermi level), and resulted in the formation of Schottky barriers at the hetero-junctions [33], which acted as a rapid separation site for the photoinduced electrons and holes and improved the photocatalytic activity of Ag-TiO_2. Besides, upon UV excitation the photoinduced electrons were accumulated at Ag or lower conduction band of rutile, and were able to be transferred to the oxygen adsorbed on the surface, or holes at the valence band of anatase and rutile to form O_2^- or O_2^{2-} [34] and led to the production of surface hydroxyl radical •OH [32]. As a consequence, the photocatalytic activity of Ag-TiO_2 was significantly enhanced.

However, excessive Ag covered the surface of TiO_2, leading to the decreased concentration of photogenerated charge carrier and photocatalytic activity of catalysts [9]. And the photoholes in the interfacial region of the TiO_2 might be trapped by Ag particles and clusters before they reacted with toluene. This trapping effect was negligible in the low Ag doping content, while became prevailing in an excessive Ag doping content. This could be the reason that the photocatalytic activity of Ag-TiO_2 declined when the Ag/Ti molar ratio increased to above 2%. In addition, the photocatalytic activity of 4%AgWT was dropped drastically, which was probably due to the

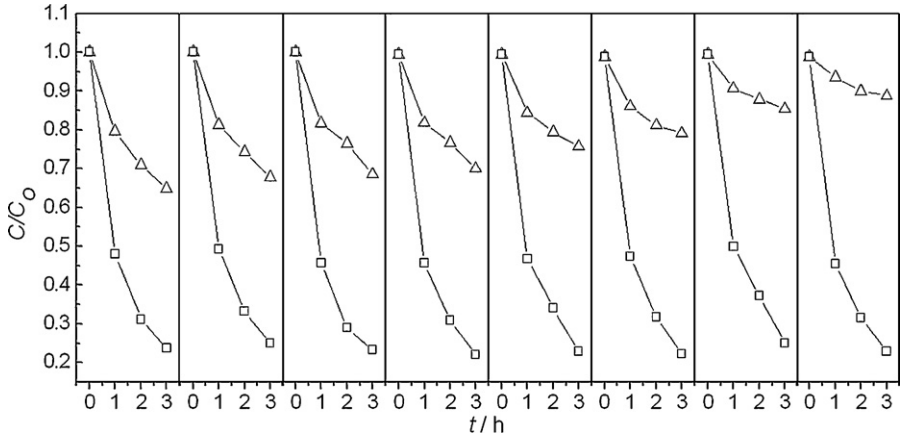

Fig. 9. Cycling runs in the photodegradation of toluene on the WT (△) and 1%AgWT (□). Catalyst powder (1.5 g); the initial concentration of toluene (9 mg/L per run).

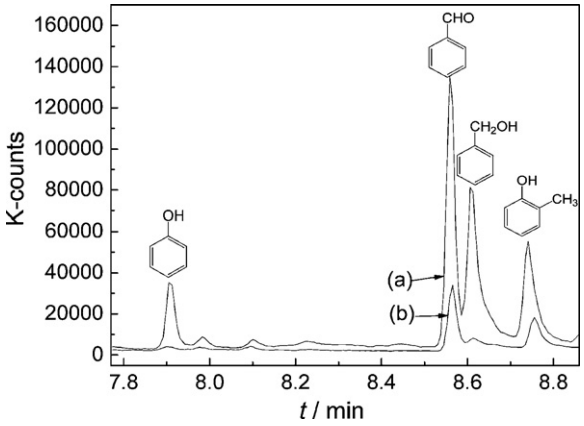

Fig. 10. Chromatogram of GC–MS analysis of the by-products adsorbed on the surface of WT (a) and 1%AgWT (b). Catalyst powder (1 g); the initial concentration of toluene (9 mg/L per run); reaction (8 run).

presence of AgO that was harmful to the photocatalytic activity of TiO_2 [35].

3.3. Role of Ag in the photostability of Ag-TiO_2

Fig. 9 shows the durability of WT and 1%AgWT catalysts for the degradation of toluene under UV light irradiation, respectively. Compared with 1%AgWT, the photocatalytic activity of WT catalyst decreased significantly. This was probably due to the accumulation of strongly adsorbed species such as benzaldehyde and benzoic acid on the surface of TiO_2 [36]. Therefore, 1%AgWT was more effective and stable than WT.

Accumulated intermediate organic products and remaining reactant were extracted from the WT and 1%AgWT catalysts and analyzed by GC–MS. The results in Fig. 10 shows that the main by-products adsorbed on the surface of catalysts were phenol, benzaldehyde, benzyl alcohol and methyl phenol. In general, toluene was first decomposed into intermediate organic products such as benzaldehyde and benzoic acid, and then into some smaller species. The adsorption of intermediate organic products on the surface of TiO_2 was considered to be an important reason for the deactivation of TiO_2 [37]. Ollis and coworkers [38] found that the major adsorbed intermediate was benzoic acid, which was considered as a major cause of TiO_2 deactivation. Larson et al. [39] also reported that the intermediate such as benzaldehyde and benzoic acid were much more strongly bound to TiO_2 than the toluene and could deactivate the catalyst. In this work, benzoic acid was not be detected. However, it can be seen that the intensity peaks of phenol, benzaldehyde, benzyl alcohol and methyl phenol adsorbed on 1%AgWT surface were weaker than that on WT, indicating that doping TiO_2 with Ag can suppress the TiO_2 deactivation.

The decomposition of organic products on TiO_2 surface required large number of active group such as electron, hole, hydroxyl radical $^{\bullet}OH$ or O_2^-. Doping TiO_2 with Ag can increase the yield of active groups, and then improved the photocatalytic activity of TiO_2. Therefore, after UV light irradiation, the organic by-products was instantly decomposed but not adsorbed on TiO_2 surface. Compared with 1%AgWT, WT adsorbed a large amount of by-products, suggesting that the organic by-products was not decomposed completely, blocked the active sites of WT, and resulted in deactivation of WT.

4. Conclusions

In this work, silver-modified TiO_2 catalysts (Ag-TiO_2) with various Ag/Ti molar ratios were prepared by MW. The samples were characterized by XRD, TEM and UV–vis. The photocatalytic activity of all the prepared samples was tested by the photocatalytic degradation of gaseous toluene. The results are as follows.

(1) Compared with the hydrothermal method, Ag-TiO_2 with small crystallite size and high crystallinity was prepared by MW in a short time. MW offered a clean, convenient and energy efficient method of heating.
(2) Doping Ag could suppress the growth of anatase grains with the increase of Ag/Ti molar ratio from 0 to 2%. Ag could also promote the phase transformation under the low temperature. Brookite and rutile were observed when the Ag/Ti molar ratio increased to above 0.5%, while Ag and AgO appeared in the catalysts when the Ag/Ti molar ratio rose to above 2%. The absorption edge of Ag-TiO_2 was broadened to the visible region, and the band gap energy of Ag-TiO_2 decreased with the increase of the Ag/Ti molar ratio.
(3) The photocatalytic activity of Ag-TiO_2 was enhanced with the increase of Ag/Ti molar ratio from 0 to 1%, and declined with the further increase to 2%. The optimal Ag/Ti molar ratio for the photocatalytic activity of Ag-TiO_2 was 1%, with the content of anatase, rutile and brookite at 71.1, 14.5 and 14.4%, respectively. Compared with pure TiO_2, Ag-TiO_2 exhibited more stable photocatalytic activity in the degradation of toluene.

Acknowledgements

This work was financially supported by the key project of Science and Technology of Hubei Province (No. 2006AA305A02). We also gratefully acknowledge the support of Analytical and Testing Center of Huazhong University of Science and Technology for the characterization of catalysts and the help of Dr. Zhang Jindong and Yuan Songhu in English writing.

References

[1] M.R. Hoffmann, S.T. Martin, W. Chio, D.W. Bahnemann, Environmental applications of semiconductor photocatalysis, Chem. Rev. 95 (1995) 69–96.
[2] A.L. Linsebigler, G. Lu, J.Y. Yates, Photocatalysis on TiO_2 surfaces: principles, mechanisms, and selected results, Chem. Rev. 95 (1995) 735–758.
[3] A. Fujishima, T.N. Rao, D.A. Tryk, Titanium dioxide photocatalysis, J. Photochem. Photobiol. C: Rev. 1 (2000) 1–21.
[4] C. Kormann, D.W. Bahnemann, M.R. Hoffmann, Preparation and characterization of quantum-size titanium dioxide, J. Phys. Chem. B 92 (1988) 5196–5201.
[5] A. Sclafani, J.M. Herrmann, Influence of metallic silver and of platinum-silver bimetallic deposits on the photocatalytic activity of titania (anatase and rutile) in organic and aqueous media, J. Photochem. Photobiol. A: Chem. 113 (1998) 181–188.
[6] C. Belver, M.J. Lopez-Munoz, J.M. Coronado, J. Soria, Palladium enhanced resistance to deactivation of titanium dioxide during the photocatalytic oxidation of toluene vapors, Appl. Catal. B: Environ. 46 (2003) 497–509.
[7] A. Dawson, P.V. Kamat, Semiconductor-metal nanocomposites. Photoinduced fusion and photocatalysis of gold-capped TiO_2 (TiO_2/gold) nanoparticles, J. Phys. Chem. B 105 (2001) 960–966.
[8] N. Sobana, M. Muruganadham, M. Swaminathan, Nano-Ag particles doped TiO_2 for efficient photodegradation of direct azo dyes, J. Mol. Catal. A: Chem. 258 (2006) 124–132.
[9] B.F. Xin, L.Q. Jing, Z.Y. Ren, B.Q. Wang, H.G. Fu, Effects of simultaneously doped and deposited Ag on the photocatalytic activity and surface states of TiO_2, J. Phys. Chem. B 109 (2005) 2805–2809.
[10] H.M. Sung-Suh, J.R. Choi, H.J. Hah, S.M. Koo, Y.C. Bae, Comparison of Ag deposition effects on the photocatalytic activity of nanoparticulate TiO_2 under visible and UV light irradiation, J. Photochem. Photobiol. A: Chem. 163 (2004) 37–44.
[11] X.Z. Li, F.B. Li, Study of Au/Au^{3+}–TiO_2 photocatalysts toward visible photooxidation for water and wastewater treatment, Environ. Sci. Technol. 35 (2001) 2381–2387.
[12] C. Hu, Y.Q. Lan, J.H. Qu, X.X. Hu, A.M. Wang, Ag/AgBr/TiO_2 visible light photocatalyst for destruction of azodyes and bacteria, J. Phys. Chem. B 110 (2006) 4066–4072.
[13] S. Rengaraj, X.Z. Li, Enhanced photocatalytic activity of TiO_2 by doping with Ag for degradation of 2,4,6-trichlorophenol in aqueous suspension, J. Mol. Catal. A: Chem. 243 (2006) 60–67.
[14] S.C. Chan, M.A. Barteau, Preparation of highly uniform Ag/TiO_2 and Au/TiO_2 supported nanoparticle catalysts by photodeposition, Langmuir 21 (2005) 5588–5595.

[15] V.G. Pol, Y. Langzam, A. Zaban, Application of microwave superheating for the synthesis of TiO_2 rods, Langmuir 23 (2007) 11211–11216.
[16] J.N. Hart, D. Menzies, Y.B. Cheng, G.P. Simon, L. Spiccia, A comparison of microwave and conventional heat treatments of nanocrystalline TiO_2, Sol. Energy Mater. Sol. Cells 91 (2007) 6–16.
[17] Z.L. Liu, B. Guo, L. Hong, H.X. Jiang, Physicochemical and photocatalytic characterizations of TiO_2/Pt nanocomposites, J. Photochem. Photobiol. A: Chem. 172 (2005) 81–88.
[18] G.M. Guo, B.B. Yu, P. Yu, X. Chen, Synthesis and photocatalytic applications of Ag/TiO_2-nanotubes, Talanta 79 (2009) 570–575.
[19] Y.B. Xie, C.W. Yuan, Visible-light responsive cerium ion modified titania sol and nanocrystallites for X-3B dye photodegradation, Appl. Catal. B: Environ. 46 (2003) 251–259.
[20] J.G. Yu, J.F. Xiong, B. Cheng, S.W. Liu, Fabrication and characterization of Ag–TiO_2 multiphase nanocomposite thin films with enhanced photocatalytic activity, Appl. Catal. B: Environ. 60 (2005) 211–221.
[21] D.M. Oman, K.M. Dugan, J.L. Killian, V. Ceekala, C.S. Ferekides, D.L. Morel, Device performance characterization and junction mechanisms in CdTe/CdS solar cells, Sol. Energy Mater. Sol. Cells 58 (1999) 361–373.
[22] Q.Y. Lu, F. Gao, S. Komarneni, Microwave-assisted synthesis of one-dimensional nanostructures, Mater. Res. 19 (2004) 1649–1655.
[23] F.K. Liu, Y.C. Chang, P.W. Huang, F.H. Ko, T.C. Chu, Preparation of silver nanorods by rapid microwave heating, Chem. Lett. 33 (2004) 1050–1051.
[24] C. He, Y. Yu, X.F. Hu, A. Larbot, Influence of silver doping on the photocatalytic activity of titania films, Appl. Surf. Sci. 200 (2002) 239–247.
[25] H.E. Chao, Y.U. Yun, H.U. Xingfang, A. Larbot, Effect of silver doping on the phase transformation and grain growth of sol–gel titania powder, J. Eur. Ceram. Soc. 23 (2003) 1457–1464.
[26] J.C. Yu, J.G. Yu, W.K. Ho, Z.T. Jiang, L.Z. Zhang, Effects of F-doping on the photocatalytic activity and microstructures of nanocrystalline TiO_2 powders, Chem. Mater. 14 (2002) 3808–3816.
[27] C. He, Y. Xiong, J. Chen, C.H. Zha, X.H. Zhu, Photoelectrochemical performance of Ag-TiO_2/ITO film and photoelectrocatalytic activity towards the oxidation of organic pollutants, J. Photochem. Photobiol. A: Chem. 157 (2003) 71–79.
[28] P.C. Maness, S. Smolinski, D.M. Blake, Z. Huang, E.J. Wolfrum, W.A. Jacoby, Bactericidal activity of photocatalytic TiO_2 reaction: toward an understanding of its killing mechanism, Appl. Environ. Microbiol. 65 (1999) 4094–4098.
[29] W.Y. Li, S. Seal, E. Megan, J. Ramsdell, K. Scammon, G. Lelong, L. Lachal, K.A. Richardson, Physical and optical properties of sol–gel nano-silver doped silica film on glass substrate as a function of heat-treatment temperature, J. Appl. Phys. 93 (2003) 9553–9561.
[30] J.H. He, I. Ichinose, T. Kunitake, A. Nakao, In situ synthesis of noble metal nanoparticles in ultrathin TiO_2-gel films by a combination of ion-exchange and reduction processes, Langmuir 18 (2002) 10005–10010.
[31] J.H. He, I. Ichinose, T. Kunitake, A. Nakao, Y. Shiraishi, N. Toshima, Facile fabrication of Ag–Pd bimetallic nanoparticles in ultrathin TiO_2-gel films: nanoparticle morphology and catalytic activity, J. Am. Chem. Soc. 125 (2003) 11034–11040.
[32] J.Y. Zheng, H. Yu, X.J. Li, S.Q. Zhang, Enhanced photocatalytic activity of TiO_2 nano-structured thin film with a silver hierarchical configuration, Appl. Surf. Sci. 254 (2008) 1630–1635.
[33] K.V.S. Rao, B. Lavedrine, P. Boule, Influence of metallic species on TiO_2 for the photocatalytic degradation of dyes and dye intermediates, J. Photochem. Photobiol. A: Chem. 154 (2003) 189–193.
[34] M. Miyauchi, A. Nakajima, K. Hashimoto, T. Watanabe, A high hydrophilic thin under 1 $\mu W/cm^2$ UV illumination, Adv. Mater. 12 (2000) 1923–1927.
[35] W.J. Wang, J.L. Zhang, F. Chen, D.N. He, M. Anpo, Preparation and photocatalytic properties of Fe^{3+}-doped Ag@TiO_2 core–shell nanoparticles, J. Colloid Interface Sci. 323 (2008) 182–186.
[36] Y. Irokawa, T. Morikawa, K. Aoki, S. Kosaka, T. Ohwaki, Y. Taga, Photodegradation of toluene over TiO_2-xN_x under visible light irradiation, Phys. Chem. Chem. Phys. 8 (2006) 1116–1121.
[37] M.C. Blount, J.L. Falconer, Steady-state surface species during toluene photocatalysis, Appl. Catal. B: Environ. 39 (2002) 39–50.
[38] M.L. Sauer, M.A. Hale, D.F. Ollis, Heterogenous photocatalytic oxidation of dilute toluene–chlorocarbon mixtures in air, J. Photochem. Photobiol. A: Chem. 88 (1995) 169–178.
[39] S.A. Larson, J.L. Falconer, Initial reaction steps in photocatalytic oxidation of aromatics, Chem. Lett. 44 (1997) 57–65.